Check for updates

A quick and versatile one step metal–organic chemical deposition method for supported Pt and Pt-alloy catalysts†

Colleen Jackson,[a] Graham T. Smith,[b] Nobuhle Mpofu,[c] Jack M. S. Dawson,[a] Thulile Khoza,[d] Caelin September,[e] Susan M. Taylor,[f] David W. Inwood, [ID][g] Andrew S. Leach,[h] Denis Kramer, [ID][i] Andrea E. Russell, [ID][j] Anthony R. J. Kucernak [ID][a] and Pieter B. J. Levecque [ID]*[c]

A simple, modified Metal–Organic Chemical Deposition (MOCD) method for Pt, PtRu and PtCo nanoparticle deposition onto a variety of support materials, including C, SiC, B_4C, LaB_6, TiB_2, TiN and a ceramic/carbon nanofiber, is described. Pt deposition using $Pt(acac)_2$ as a precursor is shown to occur *via* a mixed solid/liquid/vapour precursor phase which results in a high Pt yield of 90–92% on the support material. Pt and Pt alloy nanoparticles range 1.5–6.2 nm, and are well dispersed on all support materials, in a one-step method, with a total catalyst preparation time of ∼10 hours (2.4–4× quicker than conventional methods). The MOCD preparation method includes moderate temperatures of 350 °C in a tubular furnace with an inert gas supply at 2 bar, a high pressure (2–4 bar) compared to typical MOCVD methods (∼0.02–10 mbar). Pt/C catalysts with Pt loadings of 20, 40 and 60 wt% were synthesised, physically characterised, electrochemically characterised and compared to commercial Pt/C catalysts. TEM, XRD and *ex situ* EXAFS show similar Pt particle sizes and Pt particle shape identifiers, namely the ratio of the third to first Pt coordination numbers modelled from *ex situ* EXAFS, between the MOCD prepared catalysts and commercial catalysts. Moreover, electrochemical characterisation of the Pt/C MOCD catalysts obtained ORR mass activities with a maximum of 428 A g_{Pt}^{-1} at 0.9 V, which has similar mass activities to the commercial catalysts (80–160% compared to the commercial Pt/C catalysts).

Introduction

Platinum metal and alloy nanoparticles supported on high surface area carbon (Pt/C and Pt-M/C) are the typical electrocatalysts used for both the anode and cathode of the hydrogen polymer electrolyte membrane fuel cell (PEMFC),[1–6] as platinum is the most active metal for the hydrogen oxidation (HOR on the anode)[1,3,4] and oxygen reduction reactions (ORR on the cathode).[2,4–6] Similarly, Pt/C catalysts are used to catalyse the hydrogen evolution reaction (HER)[1,3,7,8] in PEM water electrolysers, as well as in electrochemical hydrogen compressors which utilise the hydrogen oxidation and evolution reactions to purify and compress hydrogen[9] for fuel cell electric vehicle re-fuelling stations. Furthermore, alternative Pt support materials to carbon, in order to prevent the loss of Pt surface area due to carbon corrosion causing dissolution/agglomeration of Pt nanoparticles, is a prevalent research topic.[10–16] Additionally, strong metal support interactions (SMSIs) between the Pt and alternative support materials have been shown to increase the electrochemical activity of Pt through electronic, charge transfer effects.[10,11,17–23]

As the infrastructure for the hydrogen economy grows, due to a recent emphasis on renewable, clean energy sources, so does the need for large scale-up and optimisation of the Pt nanoparticle synthesis method. Moreover, alternative support materials require considerable efforts to improve the Pt utilisation, conductivity, porosity, surface area and corrosion resistance of the support[24] in order to increase the commercialisation of these catalysts. Thus, a reliable, versatile and quick Pt deposition method is desirable for the current, commonly

[a]*Department of Chemistry, Imperial College London, Imperial College Road, London, SW7 2AZ, UK*

[b]*National Physical Laboratory, Hampton Road, Teddington, TW11 0LW, UK*

[c]*HySA/Catalysis, Centre for Catalysis Research, Department of Chemical Engineering, University of Cape Town, Rondebosch, 7701, South Africa*

[d]*SINTEF Industry, SINTEF, Trondheim, 7034, Norway*

[e]*Unilever, Boksburg East Industrial, Boksburg, 1459, South Africa*

[f]*RD Graphene, 34-35 Stirling Enterprise Park, Stirling, FK7 7RP, UK*

[g]*ZapGo Ltd. Rutherford Appleton Laboratory, Harwell, Oxford, OX11 0QX, UK*

[h]*Electrochemical Innovation Lab, University College London, London, WC1E 7JE, UK*

[i]*Faculty of Engineering and the Environment, University of Southampton, University Road, Southampton, SO17 1BJ, UK*

[j]*Department of Chemistry, University of Southampton, University Road, Southampton, SO17 1BJ, UK. E-mail: Pieter.Levecque@uct.ac.za*

† Electronic supplementary information (ESI) available. See DOI: 10.1039/d0ra03001e

used catalysts (Pt/C) as well as for Pt deposited on emerging alternative support materials.

Wet chemistry methods, namely the sodium borohydride/formate reduction[14,15,25–28] and ethylene glycol reduction (polyol method)[16,26,28–32] methods are the most commonly used synthesis methods for supported Pt nanoparticle preparation. However, these methods are time consuming (∼24–40 hours per batch) and frequently involve five steps, including (1) impregnation with mixture of precursors to form a homogenous mixture, (2) chemical reduction with a reducing agent, (3) washing, (4) drying and (5) calcination/activation at temperature.[28] An extensive washing step (3) is typically required with large volumes of de-ionised water, as contaminants are left on the catalyst surface, which may deactivate the catalyst.

Organometallic Chemical Vapour Deposition (OMCVD), also known as Metal–Organic Vapour-Phase Epitaxy (MOVPE) or Metal–Organic Chemical Vapour Deposition (MOCVD), is a vacuum deposition method which produces a thin solid film on a substrate material by a chemical reaction of vapour-phase metal–organic or organometallic precursors.[33] The precursors used in the CVD method dictate the naming of the technique, as organometallic (OM-) compounds contain one or more chemical bonds between a metal and a carbon in an organic molecule and metal–organic (MO-) compounds contain a chemical bond between a metal and an organic ligand. CVD has many advantages over wet chemical methods since it is a one-stage process, removing synthesis steps such as impregnation, washing, drying and calcination/activation. Additionally, thin-film platinum deposition using this method has been extensively studied and shown to produce materials which show good electrochemical properties for a range of electrochemical devices.[34–38]

The procedure of a traditional OMCVD/MOCVD method of metal deposition to a thin film is performed by either the injection of the vaporised precursor with an inert gas into a reactor or a liquid delivery system of the precursor and a solvent which is sprayed onto the substrate. Another method of CVD involves the precursors' decomposition in the vapour phase, contained in a reactor with an inert gas, allowing for the metal to deposit on the surface of a substrate.[39] Simply put, this CVD mechanism consists of (1) a physical van der Waals interaction between the precursor and the substrate, (2) excitation of the precursor by interactions with the atoms in the substrate and through collisions with the surface or other precursors, after repeat collisions then sufficient energy is obtained to break chemical bonds in the precursor and (3) chemisorption of the precursor reactive intermediates occurs onto the surface of the substrate.[40] The mean dissociation energy required to break the metal–oxygen bond in a β-diketonate compound is 418–481 kJ mol^{-1}.[41] After the production of reactive intermediates, now absorbed to the surface, and gaseous by-products, (4) further decomposition of the precursor occurs[40] followed by (5) surface diffusion to growth sites and nucleation leading to film formation.[33] The remaining ligand fragment by-products from the decomposition process then desorb and are transported away from the deposition substrate[33] and out of the reactor.

One experimental challenge of the OMCVD/MOCVD method, particularly for scale-up to industrial scale, is the need for a vacuum in order for the precursor to sublime or vaporise at low temperatures. The OMCVD/MOCVD conditions typically used are ∼0.02–10 mbar with temperature ranges of 100–700 °C.[33–38] The necessity of low vacuum pressures requires specialised equipment to achieve and maintain a vacuum throughout the experiment, which creates practical difficulties. One way to address this challenge is to increase the operating pressure to higher pressures, such as atmospheric pressure or above. One study by Kulbakov et al.[42] describes a two-step non-isothermal decomposition of platinum acetylacetonate (Pt(acac)$_2$) at atmospheric pressure under air to prepare size controlled Pt nanoparticles deposited on carbon which were shown to be active for ethanol electro-oxidation.

This study describes the experimental setup and description of a one-step metal–organic chemical deposition (MOCD) method, wherein which Pt deposition, to form nanoparticles, occurs from a mixed solid–liquid–vapour phase rather than purely from the vapour phase. This system operates with a 2 bar inert gas (operation pressure is between 4.6–15.3 bar if the temperature and ligand pressure is included, assuming the ideal gas law) at 350 °C, with a total preparation time of ∼10 hours, to produce Pt and Pt alloy nanoparticles dispersed on high surface area carbon and other support materials such as carbides, a nitride, borides and carbon nanofibers. Here, the versatility of this MOCD method to deposit Pt nanoparticles on carbon and on other support substrates is shown. Additionally, direct physical and electrochemical comparisons for ORR in acidic media will be made between Pt/C catalysts produced *via* this MOCD method and commercially available Pt/C catalysts.

Experimental

Catalyst synthesis

In order to remove any surface contaminants, the reactor and reactor end tubing were rinsed with 18.2 MΩ cm DI water (Milli-Q) and acetone (AR Grade Kimix), then sonicated in DI water for 30 minutes and left to dry in an oven at 90 °C for 1 hour.

Pt(acac)$_2$ (97% Sigma-Aldrich), Ru(acac)$_2$ (97% Sigma-Aldrich) and/or Co(acac)$_3$ (98% Sigma-Aldrich) was physically mixed with the desired support material. The support materials, used as-received, were Vulcan XC-72R (ElectroChem, Inc.), Silicon Carbide (NaBond Technologies Co., Ltd.),[43] LaB$_6$ (American Elements), TiB$_2$ (US Research Nanomaterials),[44,45] TiN (US Research Nanomaterials), ceramic/carbon nanofiber (Stellenbosch Nanofiber Company).[45] Boron carbide/graphite composite (BC) (NaBond Technologies Co., Ltd.) was treated with nitric acid to increase the number of nucleation sites[10,11,43] and boron doped SiC (B:SiC) and boron doped B$_4$C (B:B$_4$C) were synthesised in-house using adaptations of previously reported carbothermal synthesis methods.[46,47] Briefly, the B:SiC and B:B$_4$C preparation involved either co-polymerisation or co-precipitation of carbon, boron and silicon precursors to yield a solid homogenous precursor that was finely powdered using a bead-mill and reduced to ceramic powders by heating in argon.

After mixing, by shaking (no drying or grinding), the desired $Pt(acac)_2$ (with $Ru(acac)_2$ or $Co(acac)_3$) mass with the support material to produce a total catalyst mass, of the Pt and support ignoring the acetylacetonate contribution, of $\sim$250 mg for the $\sim$8 cm^3 (main reactor chamber is 4.2 cm in length with an inner diameter of 1.6 cm) volume reactor, the precursors were placed in the reactor[48] and the reactor was placed into a tubular furnace (Fig. 1). For the nanofibers, these were placed into a graphite weighing boat and the precursor was uniformly distributed over the fibers before being placed in the reactor and then the reactor into the furnace. Argon was fed into the reactor at a pressure of 2 bar, controlled by a pressure regulator, at room temperature while the tubular furnace was ramped to 100 °C in 30 minutes and held for 30 minutes at 100 °C. This initial temperature ramp and Ar purge removed the air from the reactor, allowed for dynamic mixing of the precursors in the reactor and also removed excess moisture from the precursors. After the initial temperature ramp and hold (1 hour), the two manual control valves, placed before (CV1-Fig. 1) and after the furnace (CV2-Fig. 1), were closed and the temperature of the furnace was ramped to 350 °C over 1 hour ($\sim$4 °C min^{-1}) and held at 350 °C for 2 hours. The reactor was then removed from the furnace, while still closed and under Ar atmosphere, and left to cool for at least 5 hours at room temperature and then placed on ice for 20 minutes before opening and removing the synthesised catalyst. The cooling of the reactor under ice before opening was a safety precaution as the catalyst, mostly when synthesising PtRu catalysts, may spontaneously combust when first exposed to air. This is due to the initial surface oxidation/passivation of Pt and Ru or oxidation of the acetylacetone ligand, an exothermic process, which may provide enough heat to combust a support material, particularly carbon. Thus, cooling down of the reactor and catalyst under ice reduced the reaction rate of the surface passivation or oxidation process.
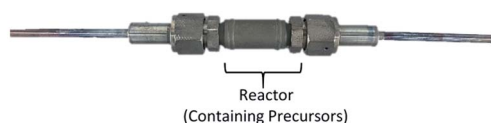

Fig. 1 Image of reactor and furnace setup, under argon atmosphere with a feed of 2 bar at room temperature, when heated to 350 °C. The manual control valves (CV1 and CV2) are open during purging ($\sim$1 h) and closed after initial purge. The quartz wool in the reactor outlet is to contain the precursors in the reactor and a beaker filled with water on the exit flow is placed while flowing Ar to monitor the gas flow and prevent air from entering the reactor.

Alternatively, passivation with humidified N_2 at 70 °C or dilute O_2 in N_2 (humidified) could be used. When O_2/N_2 was used, the O_2 concentration was slowly increased from 5–20% and kept at each combination for 10 minutes at room temperature.

The commercial Pt/C catalysts used in this study are 20 wt% Pt/C (HiSPEC 3000, Alfa Aesar and Premetek Co.), 40 wt% Pt/C (HiSPEC 4000, Alfa Aesar) and 60 wt% Pt/C (HiSPEC 9100, Alfa Aesar).

Physical characterisation

Thermogravimetric analysis (TGA) and differential thermal analysis (DTA) carried out on a Mettler Toledo TGA/SDTA851 under air and under N_2. Under air the temperature was increased with a ramp rate of 5 °C min^{-1} from 20–800 °C and under the inert atmosphere (N_2) the reactor conditions were mimicked by using a ramp rate of $\sim$3 °C min^{-1} to 100 °C then a ramp rate of $\sim$4 °C min^{-1} to 350 °C while measuring the weight and temperature of the sample.

Transmission Electron Microscopy (TEM) was performed on a Tecnai F20-FEI 200 kV + G2 electron microscope operating at 200 kV. Pt particle size was determined using an average of at least 100 Pt particle diameters from TEM images for each catalyst using ImageJ software. X-ray diffraction (Bruker D8 Advance Co Kα) was used to verify the Pt crystallite size and ICP-OES (Varian 730 ES) to confirm the Pt loading on the support.

Ex situ X-ray adsorption spectroscopy on the B18 line at the diamond light source was used to investigate the morphology of Pt on the surface of the support. The Pt L_3 (11 564 eV) edge was measured on the beamline which operated with a ring energy 3 GeV and at a current of 300 mA. The monochromator used Si(111) crystals operating in Quick EXAFS (QEXAFS) mode. A total of three spectra were averaged for each sample. The measurements were collected using the ionization chambers in transmission mode at 298 K. Calibration of the monochromator was carried out at both edges using Pt foils. These catalysts were prepared using boron nitride to bind pellets of the catalysts, the pellets were then placed under a H_2 atmosphere to reduce surface oxides and all spectra were collected at room temperature. The absorption spectra were modelled with Demeter by Bruce Ravel using Ifeffit by Matt Newville[49] to solve the EXAFS equation for the first four Pt shell co-ordination shells, as described by Frenkel *et al.*[50]

Electrochemical characterisation

A glassy carbon (GC) electrode (Pine Instruments) with 5 mm diameter was polished using 0.1, followed by 0.05 μm alumina polish (Buehler) and sonicated for 1 minute in 18.2 MΩ cm water (Millipore), 1 minute in isopropanol (VWR Chemicals) and again in 18.2 MΩ cm water (Millipore). Catalyst inks for RDE experiments were prepared with 5 mg of catalyst in 5 ml 18.2 MΩ cm water (Millipore) and 1.5 ml isopropanol (VWR Chemicals), sonicated for 30 minutes, followed by 2 : 1 ratio of carbon:Nafion® using 20 wt% Nafion® (Sigma Aldrich), and sonicated for a further 45 minutes. Finally, 10 μL of the ink was

placed on the GC electrode. The GC electrode was rotated at 700 rpm in air while the catalyst ink dried.

All glassware was cleaned in NOCHROMIX® and boiled 6 times in 18.2 MΩ cm water before testing. Electrochemical characterisations were measured in 0.1 M HClO₄ (Merck Suprapur®) electrolyte solutions at room temperature and atmospheric pressure in a three-electrode setup, utilising a hydrogen reference electrode and gold counter electrode. Cyclic voltammograms were measured in N₂ (6.8 N purity, Air Products BIP® Plus) saturated electrolytes. Electrochemical cleaning cycles were firstly done with 50 cycles and a scan rate of 100 mV s⁻¹ followed by 2 cycles at 20 mV s⁻¹ in the potential range of 0.05–1.2 V *vs.* RHE. Linear sweep voltammetry was then used to measure ORR activity in O₂ (5.8 N purity Air Products UltraPure Plus) saturated electrolyte with a potential range of −0.01 to 1 V *vs.* RHE and a scan rate of 20 mV s⁻¹, a rotation rate of 1600 rpm, for oxygen reduction activity the anodic scan was reported after iR and baseline corrections in a N₂ saturated electrolyte, as well as corrected for mass transport limitations of the setup using the Koutecký–Levich equation (eqn (1)).[51] CO stripping voltammetry was used to determine the electrochemically active surface area (ECSA), the potential was held at 0.1 V *vs.* RHE for 20 minutes in pure CO (BOC Gases) saturated electrolyte and 20 minutes in a N₂ saturated 0.1 M HClO₄ electrolyte, and cyclic voltammetry was measured with a potential range of 0.05–1.2 V *vs.* RHE with a scan rate of 20 mV s⁻¹.

$$\frac{1}{i} = \frac{1}{i_d} + \frac{1}{i_k} \tag{1}$$

The Pt/C catalyst degradation studies were completed by cycling between 0.6 and 1.0 V *vs.* RHE with a scan rate of 50 mV s⁻¹ in 0.1 M HClO₄ electrolyte solution for 6000 cycles at room temperature, and periodically reverted to a cyclic voltammogram between 0.05 and 1.2 V *vs.* RHE with a scan rate of 20 mV s⁻¹ to investigate the changes to the H_{UPD} region. The reference electrode used for the durability measurement was Hg/HgSO₄ with a gold counter electrode.

Results and discussion

Experimental setup

Images of the experimental setup is shown in Fig. 1, here a stainless-steel reactor[48] with open-close valves (CV1/2) on either side is placed into a tubular furnace. One end of the reactor is filled with quartz wool, so the contents of the reactor are contained in the reactor while argon flows through it. The gas line exiting that end of the reactor is connected to one of the open/close valves and then runs into a beaker of water to monitor gas flow. The Pt precursor and support materials are then loaded into the reactor, and the other end of the reactor is connected to an argon line at 2 bar through another open/close valve. The manual control valves are open during purging (~1 h) during the ramp to 100 °C and hold at 100 °C. Following the initial purge period, the inlet and exit valves are closed and the reactor is pressurised to 2 bar Ar.

The proposed mechanism of MOCD

The Pt(acac)₂ precursor. Platinum(II) acetylacetonate (Pt(acac)₂), a metal–organic compound, is a precursor used for the MOCVD method[34] it is a part of the β-diketonate family complexes, with the form M(CH₃COCHCOCH₃)₂, where M is the metal. In a vacuum, Pt(acac)₂ has a low vaporisation temperature of 180 °C [39] and a decomposition temperature range of 210–264 °C.[52,53]

Vaporisation and melting point of Pt(acac)₂. As noted in 'Experimental setup' section above, the inert atmosphere used is argon at an initial pressure of 2 bar. At atmospheric pressure the Pt(acac)₂ precursor has a melting point of 250 °C, this melting point is not expected to vary significantly over the pressure range of 1–4.2 bar as the volume change is small between solid and liquid phase. However, the Pt(acac)₂ liquid will also be in equilibrium with vapour, the extent of which will depend on the loading of Pt(acac)₂, the amount of decomposition, and the temperature. Using the ideal gas law equation, the pressure of the argon at the operating temperature of 350 °C is ~4.2 bar. However, the presence of both Pt(acac)₂ and (acac) ligands in the vapour phase also adds to the pressure in the reactor and this will be dependent on the Pt(acac)₂ loading. The Clausius–Clapeyron relation using constants reported for Pt(acac)₂ (eqn (2))[52] determines the vaporisation temperature of Pt(acac)₂ to be 405 °C at 4.2 bar of Pt(acac)₂ and 197 °C at 1 mbar, where the latter is similar to a reported value of 180 °C under vacuum.[39]

$$\ln(P) = 20.19 - \frac{12737}{T} \tag{2}$$

where P is pressure in atmospheres, T is temperature in kelvin, constants (20.19 and 12 737) are reported for Pt(acac)₂.[52] Between 200–350 °C, the vapourization pressure of Pt(acac)₂ is calculated to be 0.001–0.79 bar. The additional pressure due to vaporised (acac) ligands ranges from 0.37–11.1 bar for 2–60 wt% Pt catalysts, if all of the ligand vaporises and the ideal gas law is assumed.

Decomposition temperature of Pt(acac)₂. Thermogravimetric analysis (TGA) and differential thermal analysis (DTA) on Pt(acac)₂ in N₂ and air at atmospheric pressure is shown in Fig. 2. The TGA analysis is used to estimate the decomposition window of Pt(acac)₂ to determine the minimum operating temperature used in the furnace. The TGA under N₂ simulates the reactor conditions of inert atmosphere, with the same temperature ramp rate and maximum reactor temperature, to ensure full decomposition of the Pt(acac)₂ in this environment. The TGA response shows the decomposition window of Pt(acac)₂ to be between 200–320 °C as the mass of the TGA sample rapidly reduces in this temperature range. This decomposition temperature range is in agreement with the decomposition temperatures for Pt(acac)₂ in the literature of 210–264 °C.[52,53] The TGA results in Fig. 2 also show the decomposition temperature range is independent of atmosphere as the TGA response under air and N₂ are similar, where the N₂ ramp rate mimics the reactor conditions. The DTA in both atmospheres displays an endothermic response between
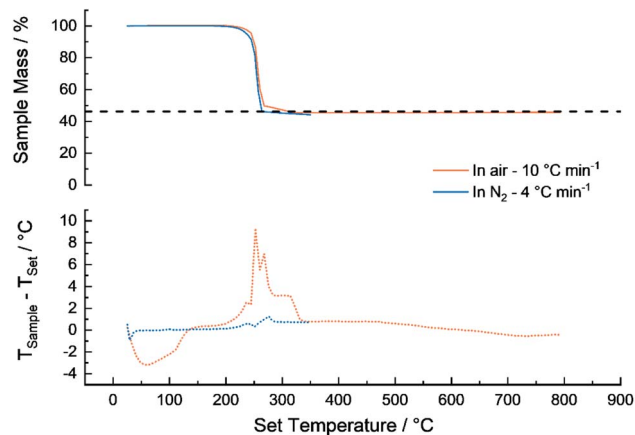
Fig. 2 Thermogravimetric analysis (top) and differential thermal analysis (bottom) on Pt(acac)$_2$ under air or N$_2$. Under air: a temperature ramp of 5 °C min^{-1} from 20–800 °C; under N$_2$: a ramp of 4 °C min^{-1} from 20–350 °C.

20–100 °C and exothermic response from 200–320 °C, attributed to water evaporation and decomposition of Pt(acac)$_2$, respectively. Both the water evaporation and Pt(acac)$_2$ decomposition in air have larger responses (approx. 7 times higher temperature differential) than under an inert N$_2$ atmosphere, indicating more energy required for the endothermic reaction and more heat produced during the exothermic decomposition reaction in air. This difference in energy requirements between an inert N$_2$ atmosphere and air is attributed to the differences in the thermal decomposition products, which will have different reaction energies, and these products vary between different atmospheres, previously investigated for O$_2$ and H$_2$ atmospheres.[40,41] When H$_2$ and O$_2$ are used, they behave as co-reactants. Under H$_2$ the ligand is likely to decompose only to H(acac), whilst O$_2$ was shown to assist in the oxidation of the ligand to different fragments (H(acac), C$_2$H$_4$, CO, and other C$_x$H$_y$O$_z$ compounds).[40,41] For the inert N$_2$ environment used in this experiment, the decomposition products are not known, however the reaction is not as exothermic so it is likely that the ligand is not oxidised to a range of fragments as documented for an O$_2$ atmosphere.

The metal loading contribution from TGA is 44.1 wt%, measured from the remaining mass, assumed to be Pt metal. The Pt mass contribution is lower than the expected 46.3 wt% Pt in Pt(acac)$_2$ (shown in the dashed line, Fig. 2). The discrepancy of ~2% is attributed to water adsorption or other organic impurities in the sample. Accordingly, since the furnace was operated at 350 °C in an Ar atmosphere, the Pt/C catalyst produced is expected to be free from organic ligand contamination.

Pt(acac)$_2$ phase during deposition and mechanism. The tabulated melting point, vaporisation pressure, decomposition temperatures and operating conditions (Table 1) shows the phase of Pt(acac)$_2$ under the operating temperature and pressure of 350 °C and 4.6–15.3 bar is difficult to determine and could be a mixture of solid, liquid, and vapour phases. The relationship between phase diagram and the decomposition

Table 1 Melting temperature (atmospheric pressure), vaporisation pressure (200–350 °C), decomposition temperature (atmospheric pressure) of Pt(acac)$_2$ and operating conditions of the setup

Transition stage	Value	Determination
Melting point	250 °C	53
Vaporisation pressure	0.001–0.79 bar	This work[a]
Decomposition temperature	200–320 °C	This work[b]
Operating conditions	350 °C, 4.6–15.3 bar	This work

[a] Calculated using the Clausius–Clapeyron relation in eqn (2). [b] Decomposition range from TGA under N$_2$.

range is also shown in Fig. 3, it can be seen that the melting point temperature of 250 °C lies between the decomposition range of 200–320 °C. However, the vaporisation pressure of 0.001–0.79 bar (calculated from eqn (2) and shown in Fig. 3) between 200–350 °C, implies that an equilibrium between the vapour and liquid phase may also exist under the operating conditions. However, the partial pressure of the Pt(acac)$_2$ is not known and thus there is insufficient evidence to determine if the vapour phase is present. Therefore, chemical vapour deposition (CVD) of Pt(acac)$_2$ under these conditions is also possible. Following the temperature profile of the reactor on the phase diagram in Fig. 3, the Pt(acac)$_2$ may undergo decomposition in all three phases (solid/liquid/vapour).

The proposed mechanism for the MOCD process (illustrated in Fig. 4), whereby metal deposition occurs from the solid/liquid/vapour phase to produce nanoparticles, is modified from the CVD process. Additionally, the reactor is a closed system whereby the precursors cannot be transported out of the system. Firstly, the proposed mechanism consists of (1) a physical van der Waals interaction between the precursor and the
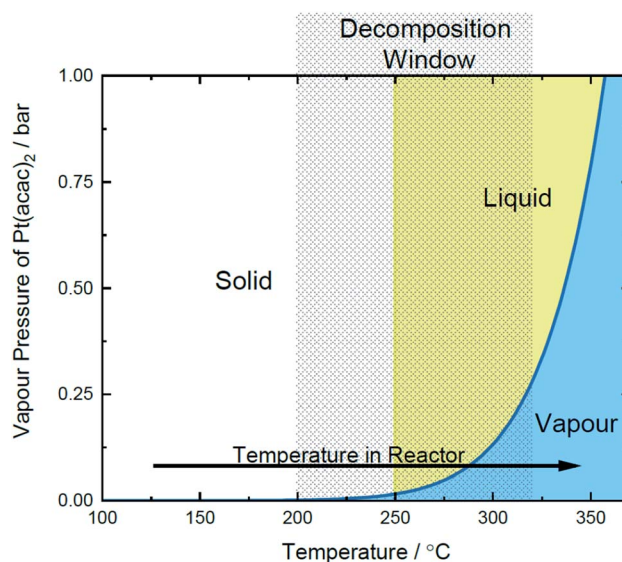

Fig. 3 Proposed Pt(acac)$_2$ phase diagram, plotted with the decomposition range and temperature excursion of the reactor.
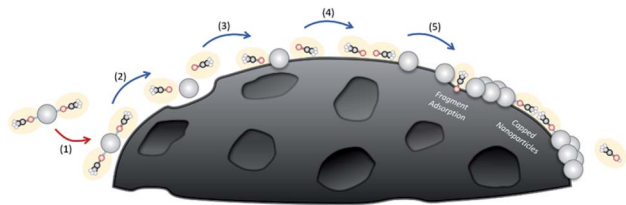
Fig. 4 Proposed Pt(acac)$_2$ deposition mechanism onto a support material, starting with decomposition of Pt(acac)$_2$, adsorption of Pt, nucleation of Pt and finally, desorption of the acetyl acetone ligand.

substrate, (2) excitation of the precursor by interactions with the atoms in the substrate from thermal energy until sufficient energy is obtained to begin to break chemical bonds in the precursor and (3) chemisorption of the precursor reactive intermediates occurs onto the surface of the substrate. (4) Further decomposition of the precursor reactive intermediates is proposed to occur from the solid/liquid/vapour phase. (5) Surface diffusion to growth sites and nucleation occurs, however, the system is closed and thus some of the remaining ligand fragment by-products will be transported away from the substrate but some may remain. In contrast to the MOCVD method, here it is proposed that some ligand fragments (H(acac), C_2H_4, CO, and other $C_xH_yO_z$ compounds) either cap the Pt nanoparticles to inhibit nanoparticle growth into Pt thin films or the ligand fragments adsorb onto the substrate and inhibit Pt nanoparticle growth by blocking surface diffusion.

Versatility of the MOCD method. Pt was deposited using the MOCD deposition method onto carbon, doped and undoped SiC, LaB$_6$, TiB$_2$, doped and undoped B$_4$C, TiN and a ceramic-carbon nanofiber (Fig. 5, 6 and Table 2), additionally, the method was previously used by one of the authors to deposit Pt onto Sb:SnO$_2$.[66] Moreover, PtRu/C and PtCo/C were synthesised and reported. The Pt particle synthesised using the MOCD deposition method were all well dispersed and consistently obtained average Pt particle sizes of <7 nm for a wide range of support materials, since Pt nanoparticle growth may be limited by the presence of ligand fragments which inhibit large particle growth or thin film growth. The particle size distributions for Pt/C MOCD prepared and commercial catalysts are shown in Fig. 6G and H, respectively, while the particle size distributions for the catalysts shown in Fig. 5, are displayed in Fig. S1.†

The Pt nanoparticle sizes reported of 2.1–2.6 nm, and particle size distributions on carbon are similar to commercial Pt/C catalysts of 2.4–2.7 nm (Fig. 6 and Table 3) and the similarities in physical properties are further discussed below under, 'Transmission electron microscopy and X-ray diffraction'. A range of Pt loadings on Pt/C were synthesised in order to fully physically and electrochemically characterise the catalysts and compare to commercial Pt/C catalysts.

The PtRu/C catalyst, typically used as anode catalysts for H$_2$ PEMFCs or Direct Methanol Fuel Cells (DMFCs) due to their CO tolerance, was synthesised using the MOCD process and produced metal nanoparticles of ∼2 nm. These PtRu particle sizes and particle size distributions are in line with previously

reported values using the conventional impregnation method with NaBH$_4$.[54,55] Further electrochemical characterisations of PtRu/C catalysts using this method were previously reported by some of us[48] which showed the operating temperature was able to control the degree of Pt–Ru alloying and PtRu particle size. Moreover, PtCo/C, an active alloy for the oxygen reduction reaction (the cathode reaction in H$_2$ PEMFCs and DMFCs), was synthesised with metal particle sizes of 1.5 nm, which is in line and/or smaller than previously reported 1.2–6.6 nm PtCo/C catalysts synthesised using different methods. The different methods used to produce PtCo/C in these studies were conventional impregnation with NaBH$_4$ (ref. 56) and iso-propanol[57] as reducing agents, and a reverse micelle method[58] which involved reduction of metal precursors with NaBH$_4$ in the presence of a surfactant, cosurfactant and oil phase. The PtCo/C particle size distribution using the MOCD method is small, spanning 0–3 nm, which is similar to PtCo/C particle sizes reported *via* the impregnation with isopropanol,[57] but significantly smaller than the PtCo/C particles produced *via* the reverse micelle method (3–7 nm) and impregnation with NaBH$_4$ (2–10 nm).[58]

The Pt nanoparticle sizes deposited on alternative support materials in this work are smaller or similar to literature values reported by other Pt deposition methods, with the exception of Pt/TiB$_2$. For the carbide support materials, Pt nanoparticle sizes of 3–8 nm were previously reported for Pt/SiC, using the pol-yol[16,60] and conventional impregnation methods (hypo-phosphite[61] and lithium formate[59] as reducing agents), which is larger than reported in this work of 2.2–3.4 nm. The particle size distribution using the MOCD method (Fig. S1†) is 2–5 nm, which is comparable to literature.[16] Moreover, Pt/BC and Pt/B:B$_4$C catalysts in this work obtain 2.3–3.4 nm Pt nanoparticles (particle size distributions between 1–4 nm for Pt/BC and 1–7 nm for Pt/B:B$_4$C), of similar range to 1.6–4.7 nm reported in literature of Pt particles prepared by the polyol method[29] and reduction of Pt(NH$_3$)$_2$(NO$_2$)$_2$ precursor in H$_2$.[62] The ORR activities for the Pt/BC catalysts were reported to show similar Pt particles and shapes to commercial Pt/C catalysts, but with significantly higher ORR activities, due to electronic metal–support interactions.[10,11]

Previous studies on boride support materials reported Pt particle sizes of 3.4 nm for Pt/TiB$_2$,[12] prepared by a colloidal method, which is smaller than the Pt particle size reported in this work of 6.2 nm, likewise, the particle size distribution reported was smaller (1–6 nm) than reported in this work of 2–11 nm. However, to our knowledge Pt/LaB$_6$ catalysts have not yet been reported in literature, using the MOCD method, the average particle size is 5.8 nm (Table 2), with a particle size distribution of 2–11 nm (Fig. S1†). Furthermore, Pt/TiN presented in this work (average of 3.9 nm and particle size distribution of 0–8 nm) is akin to literature of 3.0–6.2 nm, prepared by the polyol[63,64] and colloidal methods.[65] Reported Pt sizes of 2.9–3 nm for Pt/Sb:SnO$_2$ in literature, from particles prepared using the polyol method[67] and modified impregnation with NaBH$_4$,[68] are similar to Pt nanoparticles reported using the MOCD method.[66]
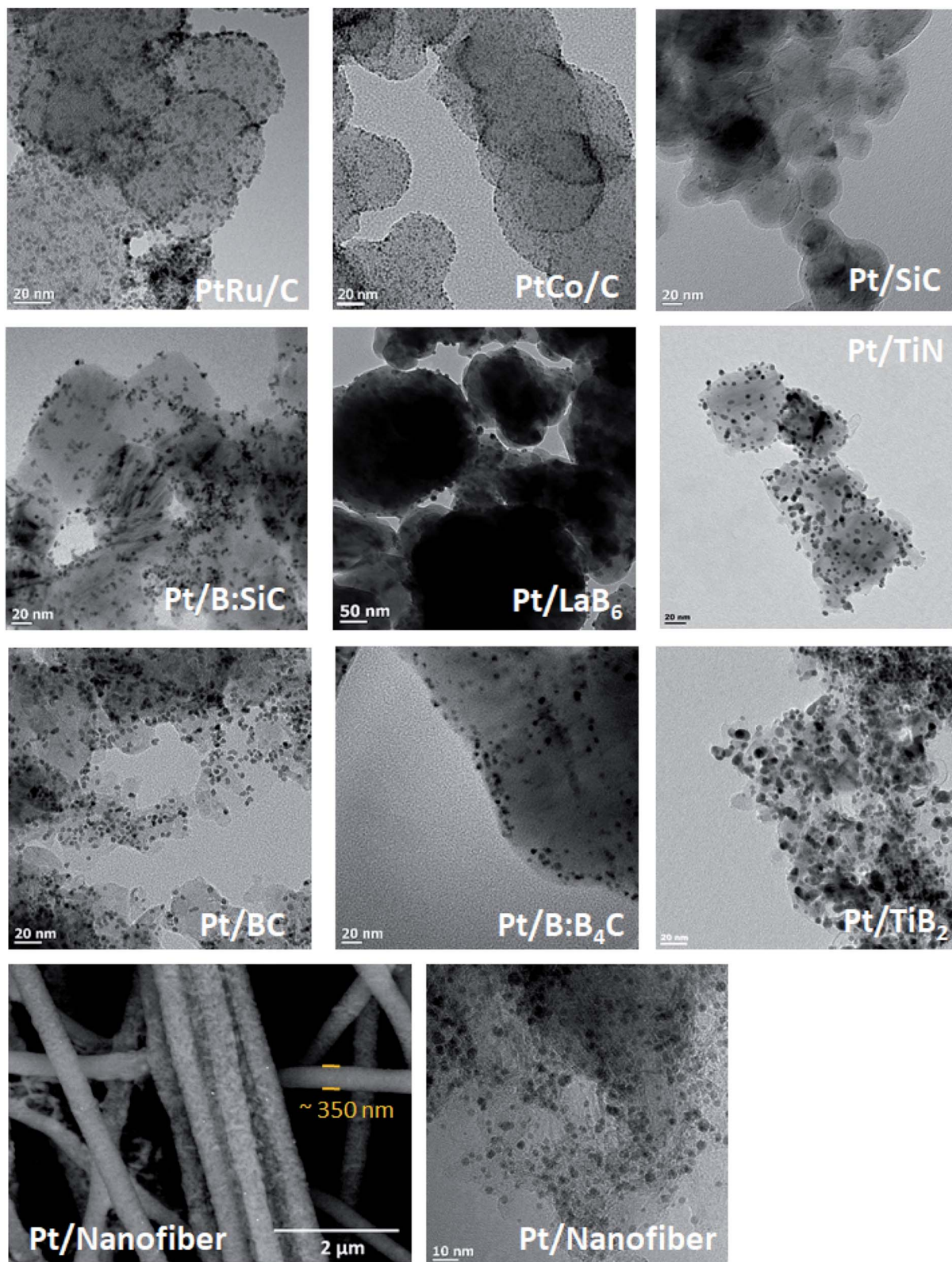
Fig. 5 Transmission Electron Microscope images of different Pt and Pt alloy nanoparticles deposited onto different support materials (as indicated on each image) using the MOCD deposition mechanism.

Finally, Pt was deposited on a ceramic-carbon nanofiber support material yielding Pt particle sizes of ~2.2 nm, which are comparable to some literature values of 2.0–3.0 nm using modified polyol methods.[69,70] The particle size distribution using the MOCD method is narrower (0–4 nm) than reported in literature by the modified polyol method (0–6 nm).[69]

Fig. 6 Transmission Electron Microscope images of MOCD prepared catalysts (A) 20 wt% Pt/C, (B) 40 wt% Pt/C, (C) 60 wt% Pt/C, and commercial catalysts (D) 20 wt% Pt/C, (E) 40 wt% Pt/C, (F) 60 wt% Pt/C, (G) MOCD Pt/C catalyst particle size distribution and (H) commercial Pt/C catalyst particle size distribution.

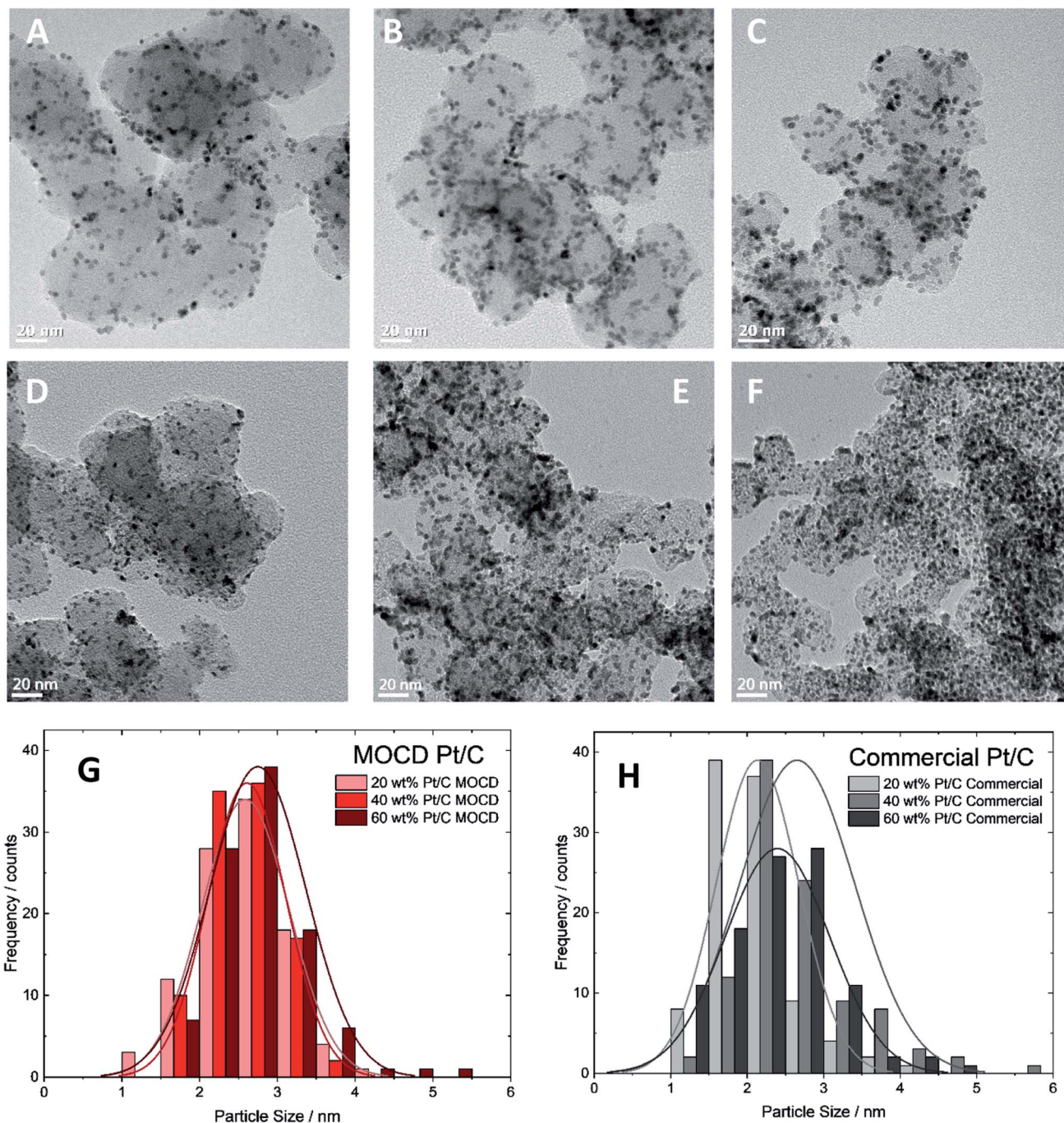### Characterisation of MOCD Pt/C catalysts

Transmission electron microscopy and X-ray diffraction. Transmission Electron Microscopy (TEM) and X-Ray Diffraction (XRD) is used to determine the platinum particle size and crystallite size, respectively. Table 3 reports the TEM Pt particle size and Pt crystallite size measured using the Scherrer equation from XRD diffraction patterns. The crystallite size (Table 3) is consistently larger than TEM particle sizes due to the lower

detection limit of XRD of ~2–2.5 nm, so particle sizes smaller than 2 nm are not identified.[71] The Pt particle and crystallite size of the metal–organic chemical deposition (MOCD) prepared Pt/C catalysts remains constant within statistical error at ~2.7 nm (TEM) and ~3.7 nm (XRD), as the platinum loading increases from 20–60 wt%. This similarity between particle size distribution and Pt loading on the MOCD catalysts is also observed in Fig. 6G, as the 20, 40 and 60 wt% MOCD prepared catalysts have

Table 2 Metal loading of Pt/Pt alloy on each support material and particle size measured from TEM images for Pt/Pt alloy catalysts synthesised using the MOCD deposition method with a comparison to reported literature Pt/Pt alloy particle sizes

Catalyst	Metal loading/wt%	MOCD TEM particle size/nm	Literature reference Pt-M particle size/nm
Pt/C	20–60	2.6–2.7	2.1–2.6[a]
PtRu/C	50	2.0 ± 0.4	1.7–4.3 (ref. 54 and 55)
PtCo/C	40	1.5 ± 0.4	1.2–6.6 (ref. 56–58)
Pt/SiC	2	2.2 ± 0.6	3.0–8.0 (ref. 16, 59–61)
Pt/B:SiC	10	3.4 ± 0.6	3.0–8.0 (ref. 16, 59–61)
Pt/LaB$_6$	8	5.8 ± 1.8	—
Pt/TiB$_2$	8	6.2 ± 2.0	3.4 (ref. 12)
Pt/BC	3–13	2.3–2.9[10]	1.6–4.7 (ref. 29 and 62)
Pt/B:B$_4$C	2	3.4 ± 1.0	1.6–4.7 (ref. 29 and 62)
Pt/TiN	8	3.9 ± 1.2	3.0–6.2 (ref. 63–65)
Pt/Sb:SnO$_2$	5–20	2.3–3.4[66]	2.9–3.0 (ref. 67 and 68)
Pt/NF	16	2.2 ± 0.7	2.0–3.0 (ref. 69 and 70)

[a] Commercial Pt/C catalysts used as a reference for MOCD Pt/C catalysts.

very similar particle size distributions. The average Pt particle size measured from TEM on the Pt/C commercial catalysts is ~2.4 nm and is independent of Pt loading. However, the Pt crystallite sizes on the commercial catalysts show an increase in Pt nanoparticle size as the Pt loading increases. The discrepancy in particle size and crystallite size on the commercial catalysts indicates a wide range of platinum particle sizes and inconstant deposition of these Pt particles which was not present in the TEM images. Furthermore, Fig. 7 displays the XRD patterns for the Pt/C commercial and MOCD prepared catalysts, the inset for Fig. 7A shows the Pt(111) peaks are similar for all MOCD catalysts with different Pt loadings while the inset of Fig. 7B shows the Pt(111) peaks are Pt loading dependant. As the Pt loading increases, the commercial catalysts' Pt(111) peak becomes narrower indicating larger Pt particle sizes, as represented in the reported Pt crystallite sizes (Table 3). This relationship is also observed in the particle size distributions (Fig. 6H), however, the MOCD prepared and commercial Pt/C catalysts' particle size distributions are within the range of 1–6 nm (compare Fig. 6G and H).

These XRD crystallite sizes may be compared to previously reported Pt/C catalysts using the MOCD method by some of the authors,[72] Pt crystallite sizes of 3.4–4.6 nm for 20, 40 and 60 wt% Pt/C catalysts were reported, which are similar to the XRD

crystallite sizes shown here of ~3.6–4.1 nm. This indicates good reproducibility of the technique between batches when using the MOCD method for Pt deposition.

One issue observed with the MOCVD method is carbon contamination of the metal thin film layers by the fragments of the ligand during deposition.[40] In order to confirm that carbon was not a significant contaminant in the Pt nanoparticles produced by the MOCD method, the Pt *d*-spacing as determined by XRD, was compared to the commercial Pt/C catalysts (Table S1†). This shows that the MOCD prepared Pt/C catalysts have *d*-spacing's of 1.38–1.39 Å which is the same as the commercial catalysts, thus carbon is likely not incorporated into the Pt lattice and not a contaminant in the prepared Pt nanoparticles.

Platinum catalyst yield using MOCD method. The Pt loading on the catalysts ($m_{Pt, product}$) was determined by ICP-OES and the yield is determined by eqn (3), where $m_{Pt\ from\ Pt(acac)_2}$ is the Pt weight in the Pt(acac)$_2$ precursor placed into the reactor. The calculated yield (Table 4) is 88–90%, demonstrating the high utilisation of the Pt precursor. This high utilisation and yield are likely due to the solid/liquid deposition phases, as less catalyst is lost in the vapour phase and deposited on the walls of the reactor. Additionally, less catalyst is lost compared to the traditional wet chemistry method as fewer steps are required, which reduces contact losses, and no washing steps are required, reducing losses on and through the filter paper. Moreover (as seen in Fig. 2), an additional loss of ~2 wt% in expected Pt loading due to precursor impurities or water is reported, thus the actual Pt yield is closer to 90–92%. The remaining Pt could have deposited on the walls of the reactor or this loss is from error in the ICP-OES measurement.

$$\text{Yield} = \frac{m_{Pt,\ product}}{m_{Pt\ from\ Pt(acac)_2}} \quad (3)$$

Table 3 TEM particle size and XRD crystallite sizes of MOCD prepared and commercial Pt/C catalysts, with varied platinum loadings

Catalyst	TEM particle size/nm	XRD crystallite size/nm
MOCD 20 wt% Pt/C	2.6 ± 0.6	3.67 ± 0.3
MOCD 40 wt% Pt/C	2.6 ± 0.5	3.60 ± 0.1
MOCD 60 wt% Pt/C	2.7 ± 0.6	4.08 ± 0.2
Commercial 20 wt% Pt/C	2.1 ± 0.5	3.37 ± 0.2
Commercial 40 wt% Pt/C	2.7 ± 0.7	3.49 ± 0.2
Commercial 60 wt% Pt/C	2.4 ± 0.7	5.83 ± 0.6

Ex situ **X-ray absorption spectroscopy.** Pt L$_3$ *Ex situ* Extended X-ray Absorption Fine Structure (EXAFS) was used to provide further insight regarding morphology of the supported Pt particles. EXAFS was collected for the 20 wt%, 40 wt% and
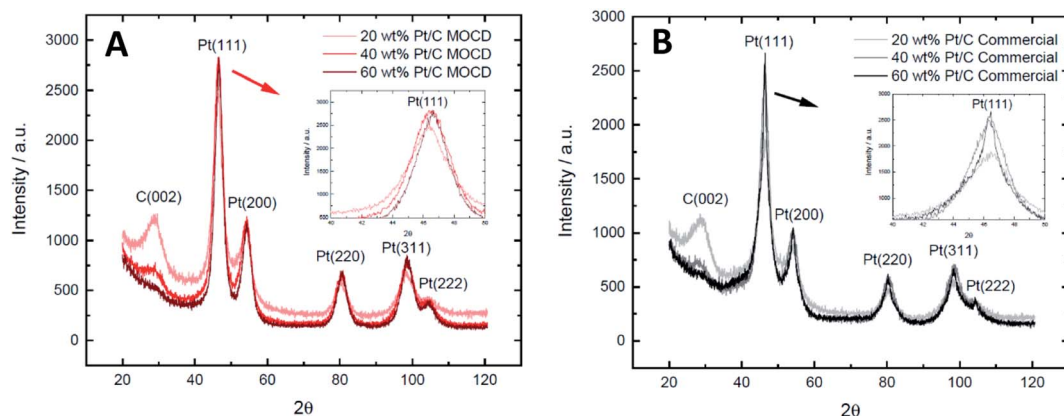
Fig. 7 X-ray diffraction patterns of the (A) 20, 40 and 60 wt% Pt/C MOCD catalysts and (B) 20, 40 and 60 wt% Pt/C commercial catalysts, showing the carbon (002) and Pt(111), (200), (220), (311) and (222) peaks with an inset of Pt(111) for each set of catalysts.

Table 4 The intended and measured Pt loading on the carbon support, used to determine the Pt yield for the MOCD method

Catalyst	Intended Pt loading/wt%	Measured Pt loading/wt%	Yield/%
MOCD 20 wt% Pt/C	20	17.7	88.4
MOCD 40 wt% Pt/C	40	35.9	89.7
MOCD 60 wt% Pt/C	60	53.5	89.2

60 wt% Pt/C MOCD and commercial catalysts (Fig. S2†). The first to fourth coordination numbers (N_1–N_4) for each of the catalysts are shown in Table S2–S4.† The first shell coordination number is strongly related to the average particle size[50] and this trend is reflected in the data, as the Pt particle sizes on the MOCD catalysts are slightly larger than the commercial catalysts, the N_1 is also larger for these catalysts. The ratio of the third to first coordination number is also an indication of particle shape.[73] The N_3/N_1 ratios are similar, between 0.93 and 1.2, for both the MOCD prepared and commercial catalysts, indicating similar particle shapes.

Electrochemical characterisation. The electrochemical characterisations of the MOCD and commercial catalysts done were CO stripping voltammetry (Fig. S4†) to determine the ECSA and ORR activities (Table 5) where measured using the rotating disc electrode. The ORR activities were normalised for mass transport limitations (eqn (1)), mass and specific surface area. The Tafel plots from ORR specific activities are shown in Fig. 8, and ORR LSVs are reported in Fig. S3.† The ECSA and ORR mass activity (0.9 V RHE, 0.1 M $HClO_4$) of the 40 wt% Pt/C commercial (HiSPEC 4000) is benchmarked in literature as 49 m^2 g^{-1} and 359 ± 14 A g$_{Pt}^{-1}$,[74] respectively, which is similar to the values reported in this work for the same commercial catalyst of 52 m^2 g^{-1} and 328 ± 43 A g$_{Pt}^{-1}$.[1] The ECSAs of all of the Pt/C catalysts, commercial and MOCD prepared, fall between the expected region for 2–5 nm Pt particle sizes.[75]

Pt particle size has a significant effect on the ORR activity as larger Pt particle sizes are more active for ORR due to the shape dependence of the Pt facets and edges ratio, with larger particles having a greater proportion of surface area associated with the more ORR active facets. This leads to an increase in specific activity but lower mass activity as the Pt utilisation is decreased with increasing Pt particle size[72,76] at 0.9 V. Additionally, the Pt loading effects the H_2O_2 desorption–readsorption reaction mechanism during the ORR,[72] thus low Pt loading catalysts will produce more H_2O_2 (two electron process) than higher loadings. The particle size and Pt loading effects are prevalent in the ORR mass and specific activities between catalysts with the same Pt loading reported in Table 5. The 40 wt% Pt/C MOCD catalyst has a higher ECSA which indicates smaller Pt particle

Table 5 Electrochemically active surface area (ECSA) measured from CO stripping voltammetry, ORR mass activity and ORR specific activity at 0.9 V vs. RHE for the MOCD and commercial catalysts, error bars from three electrodes and electrochemical characterisations. ORR activity measured in O_2 saturated 0.1 M $HClO_4$ electrolyte at room temperature with a scan rate of 20 mV s^{-1} and baseline corrected in N_2 saturated 0.1 M $HClO_4$

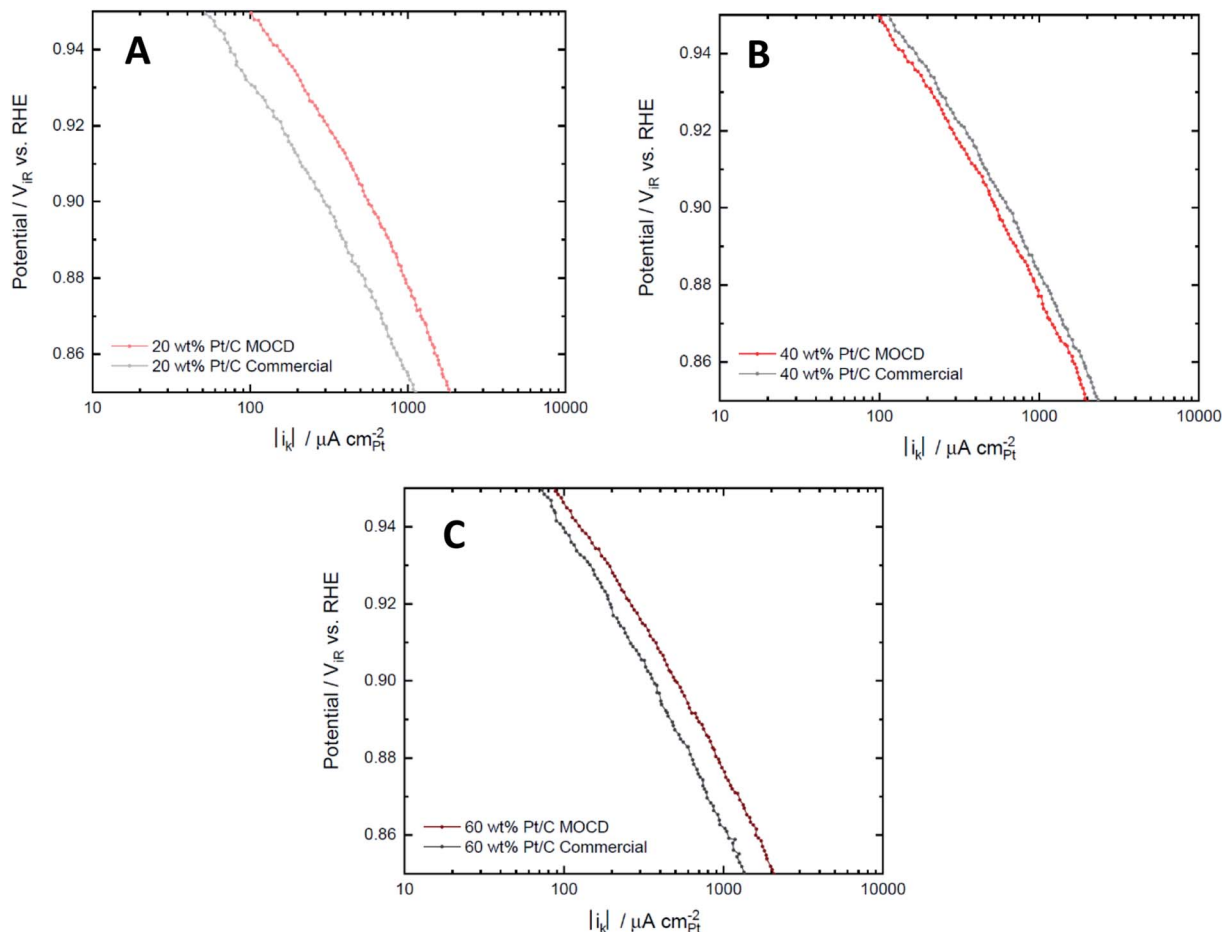| Catalyst	ECSA/m^2 g$_{Pt}^{-1}$	Mass activity/A g$_{Pt}^{-1}$	Specific activity/μA cm$_{Pt}^{-1}$
MOCD 20 wt% Pt/C	75.4 ± 3.2	426 ± 33	564 ± 26
MOCD 40 wt% Pt/C	62.7 ± 0.5	339 ± 52	541 ± 78
MOCD 60 wt% Pt/C	42.6 ± 0.8	206 ± 19	485 ± 52
Commercial 20 wt% Pt/C	76.6 ± 3.6	271 ± 36	354 ± 46
Commercial 40 wt% Pt/C	52.2 ± 3.2	328 ± 43	627 ± 66
Commercial 60 wt% Pt/C	65.8 ± 3.3	256 ± 15	390 ± 29

Fig. 8 Tafel plots of ORR specific activity for (A) 20 wt%, (B) 40 wt% and (C) 60 wt% MOCD and commercial Pt/C catalysts (HiSPEC 3000 for 20 wt% Pt/C) measured in O_2 saturated 0.1 M $HClO_4$ electrolyte at room temperature with a scan rate of 20 mV s^{-1}.

sizes, leading to a comparably higher mass activity and lower specific activity compared to the commercial 40 wt% Pt/C catalyst. Likewise, the ECSA of the 60 wt% Pt/C MOCD catalyst is lower than the commercial 60 wt% Pt/C catalyst which indicates larger Pt particle sizes, leading to a comparably lower mass activity and higher specific activity compared to the commercial 60 wt% Pt/C catalyst. The 20 wt% catalysts, however, deviate from this trend as the 20 wt% Pt/C MOCD prepared catalyst has higher mass and specific ORR activities compared to the 20 wt% Pt/C commercial catalyst, likely due to the low loading and small Pt particle sizes of the commercial catalyst leading to production of hydrogen peroxide, favouring the two electron oxygen reduction mechanism over the preferred four electron reduction mechanism.[72] An electrochemical characterisation with a second commercial catalyst (20 wt% Pt/C from Premetek Co.) reported in Table S5,† demonstrates similar ORR activities between the 20 wt% MOCD prepared and 20 wt% Pt/C (Premetek Co.). The CO Stripping voltammograms (Fig. S4†) for the 20 wt% catalysts also show similarities in peak height and position between the 20 wt% MOCD prepared and 20 wt% Pt/C Premetek Co. catalyst, indicating similar particle sizes and Pt facets. Finally, the Tafel plots of the different Pt loadings for the MOCD prepared and

commercial catalysts reported in Fig. 8 show similar ORR specific activities between the MOCD and commercial catalysts, with the exception of 20 wt% Pt/C commercial since the MOCD catalyst has a significantly higher activity.

Table 6 reports the comparison between the Pt/C MOCD prepared catalysts and commercial catalysts, showing the ORR mass activities and specific activities of the MOCD catalysts range 80–157% and 86–159% of the commercial catalysts' activity, respectively. Therefore, it can be seen that this simple one-step MOCD method can be used to produce electrochemically active Pt/C catalysts which perform similarly to or better than commercial Pt/C catalysts for oxygen reduction.

Table 6 Comparison between ECSAs, ORR mass activity and ORR specific activity at 0.9 V vs. RHE between the MOCD and commercial catalysts

Catalyst	$\dfrac{ECSA_{MOCD}}{ECSA_{Commercial}}$/%	$\dfrac{i_{m,\ MOCD}}{i_{m,\ Commercial}}$/%	$\dfrac{i_{k,\ MOCD}}{i_{k,\ Commercial}}$/%
20 wt% Pt/C	98.4	157	159
40 wt% Pt/C	120	103	86.3
60 wt% Pt/C	64.7	80.4	124

Additionally, the durability after potential cycling from 0.6–1.0 V (displayed in Fig. S5†), shows similar ECSAs between the MOCD and commercial Pt/C catalysts after 6000 cycles. The potential range of 0.6–1 V isolates the Pt chemical and electrochemical stability,[77] indicating further that the Pt/C MOCD and commercial catalysts are similar in chemical and electrochemical response.

Moreover, the versatility and reproducibility of the MOCD method allows for novel Pt catalysts and electrocatalysts to be developed in a simple and reliable manner.

Conclusion

The experimental setup and method of the MOCD catalyst preparation is described, utilising a stainless steel reactor in a tubular furnace. The operating temperature of the furnace is 350 °C and argon gas is fed into the reactor with a pressure of 2 bar at room temperature, which results in an operating pressure of 4.6–15.3 bar, if the ideal gas law is assumed and the additional ligand pressure is included. This Pt deposition method is advantageous since it is an ergonomic, one-step method, compared to wet chemistry which is typically five steps. The MOCD method may also be easily scaled up to larger reactors and batch sizes. Additionally, the use of $Pt(acac)_2$ as a precursor does not introduce chloride species into the procedure, which may act as a contaminant in the final Pt/C product.

The experimental setup and deposition method is modified from the MOCVD/OMCVD method wherein which deposition occurs from the vapour phase under vacuum in order to produce Pt thin-films on a substrate. By operating under higher pressure rather than a vacuum and in a closed reactor the $Pt(acac)_2$ precursor will decompose from a mixture of solid/liquid/vapour phases. In contrast to the MOCVD/OMCVD method, small well dispersed Pt nanoparticles with particle sizes of 1.5–6.2 nm are prepared. It is postulated that $Pt(acac)_2$ decomposition and deposition from the liquid and vapour phases allows for the good dispersion on the support material.

A mechanism is proposed for the MOCD process, this consists of (1) a physical van der Waals interaction between the precursor and the substrate, (2) excitation of the precursor by interactions with the atoms in the substrate and thermal energy until sufficient energy is obtained to break chemical bonds in the precursor and (3) chemisorption of the precursor reactive intermediates onto the surface of the substrate. (4) Decomposition and adsorption of the precursor reactive intermediates from the solid/liquid/vapour phase. (5) Surface diffusion to growth sites and nucleation occurs. Since the system is closed, the remaining ligand fragment by-products cannot be transported away from the substrate as they would be in traditional MOCVD. Here in the MOCD method, it is proposed that ligand fragments (H(acac), C_2H_4, CO, and other $C_xH_yO_z$ compounds) either cap the Pt nanoparticles to inhibit nanoparticle growth or the ligand fragments adsorb onto the substrate and inhibit Pt nanoparticle growth by blocking surface diffusion.

The MOCD deposition method was used to deposit Pt nanoparticles onto a range of support materials, specifically carbon, silicon carbide (doped and undoped), boron carbide (doped and undoped), lanthanum hexaboride, titanium diboride, titanium nitride and a ceramic/carbon nanofiber. Furthermore, a Pt alloy catalysts were also prepared and all MOCD prepared catalysts produced well dispersed Pt/Pt alloy nanoparticle sizes (1.5–6.2 nm) similar to commercial catalysts and to other literature for Pt supported on alternative materials (carbides, borides, nitrides etc.). Thus, the flexibility of the MOCD technique is demonstrated to prepare, in a one-step method, a number of Pt and Pt alloy catalysts supported on various materials with a reliable nanoparticle size range. The reproducibility of the MOCD technique is shown in the number of different supported Pt/Pt alloy catalysts produced by the technique, which have similar Pt particle sizes, particle size distributions and particle shapes. Additionally, the crystallite sizes of Pt/C catalysts are consistent with previously reported work by some of the authors, indicating reproducibility between batches.

Three Pt/C catalysts with different Pt loadings of 20, 40 and 60 wt% were physically and electrochemically characterised and compared to commercial Pt/C catalysts with similar loadings. A high Pt yield of 90–92% of the nominal loading was found for the Pt/C MOCD synthesised catalysts, demonstrating that little precursor is lost during preparation method. While slight differences in Pt particle sizes were observed from TEM and XRD between the MOCD and commercial catalysts, both sets of Pt catalysts' average particle size ranged from 2–3 nm. The first coordination number modelled from *ex situ* EXAFS was predominantly influenced by the Pt particle size and resembled this in slightly larger first coordination numbers for Pt/C catalysts with larger Pt nanoparticle sizes. Additionally, a shape identifier from *ex situ* EXAFS, the ratio of the third to first Pt coordination numbers, demonstrated that the MOCD prepared and commercial Pt/C catalyst were similar in shape. ORR mass activities and specific activities reported are 200–430 A g_{Pt}^{-1} and 485–565 μA cm_{Pt}^{-1}, respectively, for the MOCD catalysts which equates to ∼80–160% of the ORR mass and specific activities measured on the commercial catalysts. These ORR activities demonstrate that the MOCD Pt deposition technique produces well dispersed, electrochemically active Pt catalysts which are comparable to commercial standards.

Conflicts of interest

There are no conflicts to declare.

Acknowledgements

References

1 J. Zhang, *PEM Fuel Cell Electrocatalysts and Catalyst Layers: Fundamentals and Applications*, Springer London, 2008.

2 B. G. Pollet, S. S. Kocha and I. Staffell, Current status of automotive fuel cells for sustainable transport, *Curr. Opin. Electrochem.*, 2019, **16**, 90–95.

3 J. Durst, C. Simon, A. Siebel, P. J. Rheinländer, T. Schuler, M. Hanzlik, J. Herranz, F. Hasché and H. A. Gasteiger, Hydrogen Oxidation and Evolution Reaction (HOR/HER) on Pt Electrodes in Acid *vs.* Alkaline Electrolytes: Mechanism, Activity and Particle Size Effects, *ECS Trans.*, 2014, **64**, 1069–1080.

4 E. Antolini, J. R. C. Salgado and E. R. Gonzalez, The stability of Pt–M (M = first row transition metal) alloy catalysts and its effect on the activity in low temperature fuel cells: a literature review and tests on a Pt–Co catalyst, *J. Power Sources*, 2006, **160**, 957–968.

5 J. Greeley, I. E. L. Stephens, A. S. Bondarenko, T. P. Johansson, H. A. Hansen, T. F. Jaramillo, J. Rossmeisl, I. Chorkendorff and J. K. Nørskov, Alloys of platinum and early transition metals as oxygen reduction electrocatalysts, *Nat. Chem.*, 2009, **1**, 552–556.

6 J. K. Nørskov, J. Rossmeisl, A. Logadottir, L. Lindqvist, J. R. Kitchin, T. Bligaard and H. Jónsson, Origin of the Overpotential for Oxygen Reduction at a Fuel-Cell Cathode, *J. Phys. Chem. B*, 2004, **108**, 17886–17892.

7 J. K. Nørskov, T. Bligaard, A. Logadottir, J. R. Kitchin, J. G. Chen, S. Pandelov and U. Stimming, Trends in the Exchange Current for Hydrogen Evolution, *J. Electrochem. Soc.*, 2005, **152**, J23–J26.

8 W. Sheng, H. A. Gasteiger and Y. Shao-Horn, Hydrogen Oxidation and Evolution Reaction Kinetics on Platinum: Acid *vs.* Alkaline Electrolytes, *J. Electrochem. Soc.*, 2010, **157**, B1529–B1536.

9 K. Fishel, G. Qian, G. Eisman and B. C. Benicewicz, Electrochemical Hydrogen Pumping, in *High Temperature Polymer Electrolyte Membrane Fuel Cells: Approaches, Status, and Perspectives*, ed. Q. Li, D. Aili, H. A. Hjuler and J. O. Jensen, Springer International Publishing, Cham, 2016; pp. 527–540.

10 C. Jackson, G. T. Smith, D. W. Inwood, A. S. Leach, P. S. Whalley, M. Callisti, T. Polcar, A. E. Russell, P. Levecque and D. Kramer, Electronic metal–support interaction enhanced oxygen reduction activity and stability of boron carbide supported platinum, *Nat. Commun.*, 2017, **8**, 15802.

11 C. Jackson, G. T. Smith, M. Markiewicz, D. W. Inwood, A. S. Leach, P. S. Whalley, A. R. Kucernak, A. E. Russell, D. Kramer and P. B. J. Levecque, Support induced charge transfer effects on electrochemical characteristics of Pt nanoparticle electrocatalysts, *J. Electroanal. Chem.*, 2018, **819**, 163–170.

12 S. Yin, S. Mu, H. Lv, N. Cheng, M. Pan and Z. Fu, A highly stable catalyst for PEM fuel cell based on durable titanium diboride support and polymer stabilization, *Appl. Catal., B*, 2010, **93**, 233–240.

13 T. Ioroi, Z. Siroma, N. Fujiwara, S. Yamazaki and K. Yasuda, Sub-stoichiometric titanium oxide-supported platinum electrocatalyst for polymer electrolyte fuel cells, *Electrochem. Commun.*, 2005, **7**, 183–188.

14 S. Huang, P. Ganesan, S. Park and B. N. Popov, Development of a Titanium Dioxide-Supported Platinum Catalyst with Ultrahigh Stability for Polymer Electrolyte Membrane Fuel Cell Applications, *J. Am. Chem. Soc.*, 2009, **131**, 13898–13899.

15 S. Huang, P. Ganesan and B. N. Popov, Electrocatalytic activity and stability of niobium-doped titanium oxide supported platinum catalyst for polymer electrolyte membrane fuel cells, *Appl. Catal., B*, 2010, **96**, 224–231.

16 H. Lv, S. Mu, N. Cheng and M. Pan, Nano-silicon carbide supported catalysts for PEM fuel cells with high electrochemical stability and improved performance by addition of carbon, *Appl. Catal., B*, 2010, **100**, 190–196.

17 T. Li, J. Qian, Q. Zhou, J. Lin and Y. Zheng, A pyrene-modified cobalt salophen complex immobilized on multiwalled carbon nanotubes acting as a precursor for efficient electrocatalytic water oxidation, *Dalton Trans.*, 2017, **46**, 13020–13026.

18 X. Wang, Z. Ma, L. Chai, L. Xu, Z. Zhu, Y. Hu, J. Qian and S. Huang, MOF derived N-doped carbon coated CoP particle/carbon nanotube composite for efficient oxygen evolution reaction, *Carbon*, 2019, **141**, 643–651.

19 S. Mandegarzad, J. B. Raoof, S. R. Hosseini and R. Ojani, Cu-Pt bimetallic nanoparticles supported metal organic framework-derived nanoporous carbon as a catalyst for hydrogen evolution reaction, *Electrochim. Acta*, 2016, **190**, 729–736.

20 S. Zhang, Z. Xia, T. Ni, Z. Zhang, Y. Ma and Y. Qu, Strong electronic metal–support interaction of Pt/CeO₂ enables efficient and selective hydrogenation of quinolines at room temperature, *J. Catal.*, 2018, **359**, 101–111.

21 M. Sharma, N. Jung and S. J. Yoo, Toward High-Performance Pt-Based Nanocatalysts for Oxygen Reduction Reaction through Organic–Inorganic Hybrid Concepts, *Chem. Mater.*, 2018, **30**, 2–24.

22 V. C. Anitha, R. Zazpe, M. Krbal, J. Yoo, H. Sopha, J. Prikryl, G. Cha, S. Slang, P. Schmuki and J. M. Macak, Anodic TiO₂ nanotubes decorated by Pt nanoparticles using ALD: an efficient electrocatalyst for methanol oxidation, *J. Catal.*, 2018, **365**, 86–93.

23 P. S. Murphin Kumar, V. K. Ponnusamy, K. R. Deepthi, G. Kumar, A. Pugazhendhi, H. Abe, S. Thiripuranthagan, U. Pal and S. K. Krishnan, Controlled synthesis of Pt nanoparticle supported TiO₂ nanorods as efficient and stable electrocatalysts for the oxygen reduction reaction, *J. Mater. Chem. A*, 2018, **6**, 23435–23444.

24 E. Antolini and E. R. Gonzalez, Ceramic materials as supports for low-temperature fuel cell catalysts, *Solid State Ionics*, 2009, **180**, 746–763.

25 L. Xiong and A. Manthiram, Synthesis and characterization of methanol tolerant Pt/TiO$_x$/C nanocomposites for oxygen reduction in direct methanol fuel Cells, *Electrochim. Acta*, 2004, **49**, 4163–4170.

26 P. Kim, J. B. Joo, W. Kim, J. Kim, I. K. Song and J. Yi, NaBH$_4$-assisted ethylene glycol reduction for preparation of carbon-supported Pt catalyst for methanol electro-oxidation, *J. Power Sources*, 2006, **160**, 987–990.

27 S. E. Eklund and D. E. Cliffel, Synthesis and Catalytic Properties of Soluble Platinum Nanoparticles Protected by a Thiol Monolayer, *Langmuir*, 2004, **20**, 6012–6018.

28 H. Liu, C. Song, L. Zhang, J. Zhang, H. Wang and D. P. Wilkinson, A review of anode catalysis in the direct methanol fuel cell, *J. Power Sources*, 2006, **155**, 95–110.

29 H. Lv, T. Peng, P. Wu, M. Pan and S. Mu, Nano-boron carbide supported platinum catalysts with much enhanced methanol oxidation activity and CO tolerance, *J. Mater. Chem.*, 2012, **22**, 9155–9160.

30 Z. Liu, L. Hong, M. P. Tham, T. H. Lim and H. Jiang, Nanostructured Pt/C and Pd/C catalysts for direct formic acid fuel cells, *J. Power Sources*, 2006, **161**, 831–835.

31 S. Song, Y. Wang and P. K. Shen, Pulse-microwave assisted polyol synthesis of highly dispersed high loading Pt/C electrocatalyst for oxygen reduction reaction, *J. Power Sources*, 2007, **170**, 46–49.

32 Z. Liu, X. Y. Ling, X. Su and J. Y. Lee, Carbon-Supported Pt and PtRu Nanoparticles as Catalysts for a Direct Methanol Fuel Cell, *J. Phys. Chem. B*, 2004, **108**, 8234–8240.

33 AnonymousChapter 1 Overview of Chemical Vapour Deposition, in *Chemical Vapour Deposition: Precursors, Processes and Applications*, ed. A. C. Jones and M. L. Hitchman, The Royal Society of Chemistry, 2009, pp. 1–36.

34 J. R. V. Garcia and T. Goto, Chemical Vapor Deposition of Iridium, Platinum, Rhodium and Palladium, *Mater. Trans.*, 2003, **44**, 1717–1728.

35 I. K. Igumenov, N. V. Gelfond, P. S. Galkin, N. B. Morozova, N. E. Fedotova, G. I. Zharkova, V. I. Shipachev, E. F. Reznikova, A. D. Ryabtsev, N. P. Kotsupalo, V. I. Titarenko, Y. P. Dikov, V. V. Distler and M. I. Buleev, Corrosion testing of platinum metals CVD coated titanium anodes in seawater-simulated solutions, *Desalination*, 2001, **136**, 273–280.

36 T. Goto, R. Vargas and T. Hirai, Preparation of iridium and platinum films by MOCVD and their properties, *J. Phys. IV*, 1993, **03**, C3–C304.

37 G. Malandrino, R. L. Nigro and I. L. Fragalà, MOCVD of Platinum (100) Films on Random Hastelloy C276, *Chem. Vap. Deposition*, 1999, **5**, 59–61.

38 S. Barison, M. Fabrizio, G. Carta, G. Rossetto, P. Zanella, D. Barreca and E. Tondello, Nanocrystalline Pt thin films obtained *via* metal organic chemical vapor deposition on quartz and CaF$_2$ substrates: an investigation of their chemico-physical properties, *Thin Solid Films*, 2002, **405**, 81–86.

39 C. Thurier and P. Doppelt, Platinum OMCVD processes and precursor chemistry, *Coord. Chem. Rev.*, 2008, **252**, 155–169.

40 I. K. Igumenov, P. P. Semyannikov, S. V. Trubin, N. B. Morozova, N. V. Gelfond, A. V. Mischenko and J. A. Norman, Approach to control deposition of ultra thin films from metal organic precursors: Ru deposition, *Surf. Coat. Technol.*, 2007, **201**, 9003–9008.

41 I. K. Igumenov, A. E. Turgambaeva and P. P. Semyannikov, General aspects of surface chemistry of metal β-diketonates, *J. Phys. IV*, 2001, **11**, Pr3-515.

42 A. A. Kulbakov, A. B. Kuriganova, M. Allix, A. Rakhmatullin, N. Smirnova, O. A. Maslova and I. N. Leontyev, Non-isothermal decomposition of platinum acetylacetonate as a cost-efficient and Size-Controlled Synthesis of Pt/C nanoparticles, *Catal. Commun.*, 2018, **117**, 14–18.

43 C. Jackson, *SiC and B4C as Electrocatalyst Support Materials for Low Temperature Fuel Cells*, University of Cape Town, 2017.

44 T. Khoza, *Evaluation of metal nitrides and borides as alternative electrocatalyst support materials for polymer electrolyte fuel cells*, University of Cape Town, 2014.

45 C. September, *Preparation and characterisation of inorganic nanostructured support materials for polymer electrolyte fuel cells*, University of Cape Town, 2015.

46 I. Yanase, R. Ogawara and H. Kobayashi, Synthesis of boron carbide powder from polyvinyl borate precursor, *Mater. Lett.*, 2009, **63**, 91–93.

47 Y. Sugahara, Y. Takeda, K. Kuroda and C. Kato, The preparation of boron-doped silicon carbide powder by the carbothermal reduction of oxides derived from the hydrolyzed methyltriethoxysilane, *J. Non-Cryst. Solids*, 1988, **100**, 542–546.

48 C. Jackson, O. Conrad and P. Levecque, Systematic Study of Pt-Ru/C Catalysts Prepared by Chemical Deposition for Direct Methanol Fuel Cells, *Electrocatalysis*, 2017, **8**, 224–234.

49 B. Ravel and M. Newville, \it ATHENA \it ARTEMIS \it HEPHAESTUS: data analysis for X-ray absorption spectroscopy using \it IFEFFIT, *J. Synchrotron Radiat.*, 2005, **12**, 537–541.

50 A. I. Frenkel, C. W. Hills and R. G. Nuzzo, A View from the Inside: Complexity in the Atomic Scale Ordering of Supported Metal Nanoparticles, *J. Phys. Chem. B*, 2001, **105**, 12689–12703.

51 A. J. Bard and L. R. Faulkner, *Electrochemical Methods: Fundamentals and Applications*, Wiley Textbooks, 2nd edn, 2000.

52 N. B. Morozova, G. I. Zharkova, P. P. Semyannikov, S. V. Sysoev, I. K. Igumenov, N. E. Fedotova and N. V. Gelfond, Vapor pressure of precursors for CVD on the base of platinum group metals, *J. Phys. IV*, 2001, **11**, Pr3–616.

53 S. Yoda, A. Hasegawa, H. Suda, Y. Uchimaru, K. Haraya, T. Tsuji and K. Otake, Preparation of a Platinum and Palladium/Polyimide Nanocomposite Film as a Precursor of Metal-Doped Carbon Molecular Sieve Membrane *via* Supercritical Impregnation, *Chem. Mater.*, 2004, **16**, 2363–2368.

54 W. Xu, T. Lu, C. Liu and W. Xing, Nanostructured PtRu/C as Anode Catalysts Prepared in a Pseudomicroemulsion with

Ionic Surfactant for Direct Methanol Fuel Cell, *J. Phys. Chem. B*, 2005, **109**, 14325–14330.

55 Q. Lu, B. Yang, L. Zhuang and J. Lu, Anodic Activation of PtRu/C Catalysts for Methanol Oxidation, *J. Phys. Chem. B*, 2005, **109**, 1715–1722.

56 M. K. Jeon, Y. Zhang and P. J. McGinn, A comparative study of PtCo, PtCr, and PtCoCr catalysts for oxygen electro-reduction reaction, *Electrochim. Acta*, 2010, **55**, 5318–5325.

57 S. Hsu, C. Liu, H. Chen, T. Chen, C. Lai, C. Lee, J. Lee, T. Chan, L. Tsai and K. Wang, The effect of Mn addition on the promotion of oxygen reduction reaction performance for PtCo/C catalysts, *Electrochim. Acta*, 2013, **105**, 180–187.

58 Y. Qian, W. Wen, P. A. Adcock, Z. Jiang, N. Hakim, M. S. Saha and S. Mukerjee, PtM/C Catalyst Prepared Using Reverse Micelle Method for Oxygen Reduction Reaction in PEM Fuel Cells, *J. Phys. Chem. C*, 2008, **112**, 1146–1157.

59 N. N. Vershinin, V. A. Bakaev, V. I. Berestenko, O. N. Efimov, E. N. Kurkin and E. N. Kabachkov, Synthesis and properties of a platinum catalyst supported on plasma chemical silicon carbide, *High Energy Chem.*, 2017, **51**, 46–50.

60 S. M. Andersen and M. J. Larsen, Performance of the electrode based on silicon carbide supported platinum catalyst for proton exchange membrane fuel cells, *J. Electroanal. Chem.*, 2017, **791**, 175–184.

61 S. Suzuki, T. Onodera, J. Kawaji, T. Mizukami, M. Morishima and K. Yamaga, Improvement in stability of carbon support for platinum catalyst by applying silicon carbide coating, *J. Power Sources*, 2013, **223**, 79–85.

62 W. T. Grubb and D. W. McKee, Boron Carbide, a New Substrate for Fuel Cell Electrocatalysts, *Nature*, 1966, **210**, 192–194.

63 H. Nan, D. Dang and X. L. Tian, Structural engineering of robust titanium nitride as effective platinum support for the oxygen reduction reaction, *J. Mater. Chem. A*, 2018, **6**, 6065–6073.

64 Y. Zheng, J. Zhang, H. Zhan, D. Sun, D. Dang and X. L. Tian, Porous and three dimensional titanium nitride supported platinum as an electrocatalyst for oxygen reduction reaction, *Electrochem. Commun.*, 2018, **91**, 31–35.

65 K. Kakinuma, Y. Wakasugi, M. Uchida, T. Kamino, H. Uchida, S. Deki and M. Watanabe, Preparation of titanium nitride-supported platinum catalysts with well controlled morphology and their properties relevant to polymer electrolyte fuel cells, *Electrochim. Acta*, 2012, **77**, 279–284.

66 R. Mohamed, T. Binninger, P. J. Kooyman, A. Hoell, E. Fabbri, A. Patru, A. Heinritz, T. J. Schmidt and P. Levecque, Facile deposition of Pt nanoparticles on Sb-doped SnO_2 support with outstanding active surface area for the oxygen reduction reaction, *Catal. Sci. Technol.*, 2018, **8**, 2672–2685.

67 M. Dou, M. Hou, F. Wang, D. Liang, Q. Zhao, Z. Shao and B. Yi, Sb-Doped SnO_2 Supported Platinum Catalyst with High Stability for Proton Exchange Membrane Fuel Cells, *J. Electrochem. Soc.*, 2014, **161**, F1231–F1236.

68 N. R. Elezovic, V. R. Radmilovic, J. Kovac, B. M. Babic, L. Gajic-Krstajic and N. V. Krstajic, Pt nanoparticles on tin oxide based support as a beneficial catalyst for oxygen reduction in alkaline solutions, *RSC Adv.*, 2015, **5**, 15923–15929.

69 Y. Ma, S. Jiang, G. Jian, H. Tao, L. Yu, X. Wang, X. Wang, J. Zhu, Z. Hu and Y. Chen, CNx nanofibers converted from polypyrrole nanowires as platinum support for methanol oxidation, *Energy Environ. Sci.*, 2009, **2**, 224–229.

70 W. Li, M. Waje, Z. Chen, P. Larsen and Y. Yan, Platinum nanopaticles supported on stacked-cup carbon nanofibers as electrocatalysts for proton exchange membrane fuel cell, *Carbon*, 2010, **48**, 995–1003.

71 K. O'Connell and J. R. Regalbuto, High Sensitivity Silicon Slit Detectors for 1 nm Powder XRD Size Detection Limit, *Catal. Lett.*, 2015, **145**, 777–783.

72 E. Fabbri, S. Taylor, A. Rabis, P. Levecque, O. Conrad, R. Kötz and T. J. Schmidt, The Effect of Platinum Nanoparticle Distribution on Oxygen Electroreduction Activity and Selectivity, *ChemCatChem*, 2014, **6**, 1410–1418.

73 A. Jentys, Estimation of mean size and shape of small metal particles by EXAFS, *Phys. Chem. Chem. Phys.*, 1999, **1**, 4059–4063.

74 Y. Garsany, I. L. Singer and K. Swider-Lyons, Impact of film drying procedures on RDE characterization of Pt/VC electrocatalysts, *J. Electroanal. Chem.*, 2011, **662**, 396–406.

75 M. Nesselberger, S. Ashton, J. C. Meier, I. Katsounaros, K. J. J. Mayrhofer and M. Arenz, The Particle Size Effect on the Oxygen Reduction Reaction Activity of Pt Catalysts: Influence of Electrolyte and Relation to Single Crystal Models, *J. Am. Chem. Soc.*, 2011, **133**, 17428–17433.

76 K. Kinoshita, Particle Size Effects for Oxygen Reduction on Highly Dispersed Platinum in Acid Electrolytes, *J. Electrochem. Soc.*, 1990, **137**, 845–848.

77 J. Wu, X. Z. Yuan, J. J. Martin, H. Wang, J. Zhang, J. Shen, S. Wu and W. Merida, A review of PEM fuel cell durability: Degradation mechanisms and mitigation strategies, *J. Power Sources*, 2008, **184**, 104.